

The dynamics of starvation and recovery

2 Justin D. Yeakel * † ‡ §, Christopher P. Kempes † ‡, and Sidney Redner † ¶ ‡

3 *School of Natural Science, University of California Merced, Merced, CA, †The Santa Fe Institute, Santa Fe, NM, ¶Department of Physics, Boston University, Boston
4 MA, ‡Contributed equally, and §To whom correspondence should be addressed: jdyeakel@gmail.com

5 Submitted to Proceedings of the National Academy of Sciences of the United States of America

6 The eco-evolutionary dynamics of species are fundamentally
7 linked to the energetic constraints of its constituent individuals.
8 Of particular importance are the tradeoffs between reproduction
9 and the dynamics of starvation and recovery in resource-limited
10 environments. To elucidate the consequences of this tradeoff,
11 we introduce a minimal nutritional state-structured model that in-
12 corporates two classes of consumer: nutritionally replete con-
13 sumers that reproduce, and undernourished, non-reproducing
14 consumers that are susceptible to mortality. As a function of the
15 transition rates between these replete and undernourished states
16 that are determined by the presence or absence of resources,
17 the consumer populations can either undergo cyclic dynamics or
18 reach a steady state. We obtain strong constraints on starvation
19 and recovery rates by deriving allometric scaling relationships
20 and find that population dynamics subject to these constraints
21 can approach the cyclic regime but are typically driven to a steady
22 state. Moreover, we find that these rates fall within a ‘refuge’ in pa-
23 rameter space, where the probability of extinction of the consumer
24 population is minimized. Thus we identify a potential mechanism
25 that may both drive and constrain the dynamics of animal pop-
26ulations. Our model provides a natural framework that predicts
27 maximum body size for mammals by determining the relative sta-
28 bility of an otherwise homogeneous population to a mutant pop-
29 ulation with altered percent body fat. For body masses $\lesssim 10^7$ g,
30 individuals with increased energetic reserves can invade resident
31 populations, and vice versa for body mass $\gtrsim 10^7$ g, thus providing
32 a principled mechanism for a within-lineage driver of Cope’s rule.

33 foraging | starvation | reproduction

34 **Significance Statement** Energetic investment in somatic mainte-
35 nance and growth vs. reproduction directly impacts the dynamics of
36 populations among species. Here, we construct a Nutritional State-
37 structured Model (NSM) to assess the population-level effects of starv-
38 ation and recovery of a consumer population in a resource-limited en-
39 vironment, and use allometric scaling relationships for mammals to es-
40 tablish all timescales and rates. Our model reveals that mammalian
41 energetic rates minimize the probability of stochastic extinction, estab-
42 lishes dynamic bounds on mammalian body size while providing inde-
43 pendent theoretical support for the energy equivalence hypothesis, and
44 provides a mechanistic driver for the evolutionary trend towards larger
45 body size known as Cope’s rule.

46 Introduction

47 The behavioral ecology of all organisms is influenced by the en-
48 ergetic state of individuals, which directly influences how they
49 invest reserves in uncertain environments. Such behaviors are
50 generally manifested as tradeoffs between investing in somatic
51 maintenance and growth, or allocating energy towards repro-
52 duction (1–3). The timing of these behaviors responds to se-
53 lective pressure, as the choice of the investment impacts future
54 fitness (4–6). The influence of resource limitation on an or-
55 ganism’s ability to maintain its nutritional stores may lead to
56 repeated delays or shifts in reproduction over the course of an
57 organism’s life.

58 The balance between (a) somatic growth and maintenance,
59 and (b) reproduction depends on resource availability (7). For
60 example, reindeer invest less in calves born after harsh winters
61 (when the mother’s energetic state is depleted) than in calves
62 born after moderate winters (8). Many bird species invest dif-
63 ferently in broods during periods of resource scarcity compared

64 to normal periods (9, 10), sometimes delaying or even foregoing
65 reproduction for a breeding season (1, 11, 12). Even fresh-
66 water and marine zooplankton have been observed to avoid
67 reproduction under nutritional stress (13), and those that do
68 reproduce have lower survival rates (2). Organisms may also
69 separate maintenance and growth from reproduction over space
70 and time: many salmonids, birds, and some mammals return to
71 migratory breeding grounds to reproduce after one or multiple
72 seasons in resource-rich environments where they accumulate
73 nutritional reserves (14–16).

74 Physiology also plays an important role in regulating repro-
75 ductive expenditures during periods of resource limitation. The
76 data collected thus far has shown that diverse mammals (47
77 species in 10 families) exhibit delayed implantation, whereby
78 females postpone fetal development (blastocyst implantation)
79 until nutritional reserves can be accumulated (17, 18). Many
80 other species (including humans) suffer irregular menstrual cy-
81 cling and higher abortion rates during periods of nutritional
82 stress (19, 20). In the extreme case of unicellular organisms,
83 nutrition is unavoidably linked to reproduction because the nu-
84 tritional state of the cell regulates all aspects of the cell cycle
85 (21). The existence of so many independently evolved mech-
86 anisms across such a diverse suite of organisms highlights the im-
87 portance and universality of the fundamental tradeoff between
88 somatic and reproductive investment. However the general dy-
89 namic implications of these constraints are unknown.

90 Though straightforward conceptually, incorporating the en-
91 ergic dynamics of individuals (22) into a population-level
92 framework (22, 23) presents numerous mathematical obsta-
93 cles (24). An alternative approach involves modeling the
94 macroscale relations that guide somatic versus reproductive
95 investment in a consumer-resource system. For example,
96 macroscale Lotka-Volterra models assume that the growth rate
97 of the consumer population depends on resource density, thus
98 implicitly incorporating the requirement of resource availability
99 for reproduction (25).

100 In this work, we adopt an alternative approach in which we
101 explicitly account for resource limitation and the subsequent
102 effects of starvation. Namely, only individuals with sufficient
103 energetic reserves can reproduce. Such a constraint leads to
104 reproductive time lags due to some members of the population
105 going hungry and then recovering. Additionally, we incorporate
106 the idea that reproduction is strongly constrained allometrically
107 (3), and is not generally linearly related to resource density. As
108 we shall show, these constraints influence the ensuing popula-

Reserved for Publication Footnotes

tion dynamics in dramatic ways.

Nutritional state-structured model (NSM)

We begin by defining a minimal Nutritional State-structured population Model (NSM), where the consumer population is partitioned into two states: (a) an energetically replete (full) state F , where the consumer reproduces at a constant rate λ and does not die from starvation, and (b) an energetically deficient (hungry) state H , where the consumer does not reproduce but dies by starvation at rate μ . The underlying resource R evolves by logistic growth with an intrinsic growth rate α and a carrying capacity C . The rate at which consumers transition between states and consume resources is dependent on their overall abundance, the abundance of resources, the efficiency of converting resources into metabolism, and how that metabolism is partitioned between maintenance and growth purposes. In the supplement we provide a fully mechanistic model for each of these dynamics and constants, and show that the system produces a simple nondimensional form which we have described below (please see the supplement for a detailed derivation).

Consumers transition from the full state F to the hungry state H at a rate σ —the starvation rate—and also in proportion to the absence of resources ($1 - R$). Conversely, consumers recover from state H to state F at rate $\xi\rho$ and in proportion to R , where ξ represents a ratio between maximal resource consumption and the carrying capacity of the resource (please see the supplement). Resources are eaten by the consumers at rate $\rho R + \delta$, which accounts for somatic growth and maintenance for starving consumers, respectively, and at rate β by full consumers which is a constant representing maximal maintenance and somatic growth (see supplement). The NSM represents a fundamental extension of the idealized starving random walk model of foraging, which focuses on resource depletion, to include reproduction and resource replenishment (26–28), and is a more general formulation than previous models incorporating starvation (29).

In the mean-field approximation, in which the consumers and resources are perfectly mixed, their densities evolve according to the rate equations

$$\begin{aligned}\dot{F} &= \lambda F + \xi\rho RH - \sigma(1 - R)F, \\ \dot{H} &= \sigma(1 - R)F - \xi\rho RH - \mu H, \\ \dot{R} &= \alpha R(1 - R) - (\rho R + \delta)H - \beta F\end{aligned}$$

This system of nondimensional equations follows from a set of first-principle relationships for resource consumption and growth (see Supplementary Materials for a full derivation and the dimensional form). Notice that the total consumer density $F + H$ evolves according to $\dot{F} + \dot{H} = \lambda F - \mu H$. This resembles the equation of motion for the predator density in the classic Lotka-Volterra model (30), except that the resource density does not appear in the growth term. As discussed above, the attributes of reproduction and mortality have been explicitly apportioned to the full and hungry consumers, respectively, so that the growth in the total density is decoupled from the resource density.

Equation [1] has three fixed points: two trivial fixed points at $(F^*, H^*, R^*) = (0, 0, 0)$ and $(0, 0, 1)$, and one non-trivial, internal fixed point at

$$\begin{aligned}F^* &= \frac{(\sigma - \lambda)\alpha\lambda\mu^2(\mu + \xi\rho)}{A(\lambda\rho B + \mu\sigma(\beta\mu + \lambda(\delta + \rho)))}, \\ H^* &= \frac{(\sigma - \lambda)\alpha\lambda^2\mu(\mu + \xi\rho)}{A(\lambda\rho B + \mu\sigma(\beta\mu + \lambda(\delta + \rho)))}, \\ R^* &= (\sigma - \lambda)\frac{\mu}{A}.\end{aligned}$$

where $A = (\lambda\xi\rho + \mu\sigma)$ and $B = (\beta\mu\xi + \delta\lambda\xi - \lambda\mu)$. The stability of this fixed point is determined by the Jacobian matrix \mathbf{J} , where each matrix element $J_{ij} = \partial\dot{X}_i/\partial X_j$ when evaluated at the internal fixed point, and \mathbf{X} is the vector (F, H, R) . The parameters in Eq. [1] are such that the real part of the largest eigenvalue of \mathbf{J} is negative, so that the system is stable with respect to small perturbations from the fixed point. Because this fixed point is unique, it is the global attractor for all population trajectories for any initial condition where the resource and consumer densities are both nonzero.

From Eq. [2], an obvious constraint on the NSM is that the reproduction rate λ must be less than the starvation rate σ , so that R^* is positive. In fact, when the resource density $R = 0$, the rate equation for F gives exponential growth of F for $\lambda > \sigma$. The condition $\sigma = \lambda$ represents a transcritical (TC) bifurcation (31) that demarcates the physical regime from the unphysical regime where all densities become < 0 . The biological implication of the constraint $\lambda < \sigma$ has a simple interpretation—the rate at which a macroscopic organism loses mass due to lack of resources is generally much faster than the rate of reproduction. As we will discuss below, this inequality is a natural consequence of allometric constraints (3) for organisms within empirically observed body size ranges.

In the physical regime of $\lambda < \sigma$, the fixed point [2] may either be a stable node or a limit cycle (Fig. 1). In continuous-time systems, a limit cycle arises when a pair of complex conjugate eigenvalues crosses the imaginary axis to attain positive real parts (32). This Hopf bifurcation is defined by $\text{Det}(\mathbf{S}) = 0$, with \mathbf{S} the Sylvester matrix, which is composed of the coefficients of the characteristic polynomial of the Jacobian matrix (33). As the system parameters are tuned to be within the stable regime but close to the Hopf bifurcation, the amplitude of the transient but decaying cycles become large. Given that ecological systems are constantly being perturbed (34), the onset of transient cycles, even though they decay with time in the mean-field description, can increase the extinction risk (35–37).

When the starvation rate $\sigma \gg \lambda$, a substantial fraction of the consumers are driven to the hungry non-reproducing state. Because reproduction is inhibited, there is a low steady-state consumer density and a high steady-state resource density. However, if $\sigma/\lambda \rightarrow 1$ from above, the population is overloaded with energetically-replete (reproducing) individuals, thereby promoting oscillations between the consumer and resource densities (Fig. 1).

Whereas the relation between consumer growth rate λ and the starvation rate σ defines an absolute bound of biological feasibility—the TC bifurcation— σ also determines the sensitivity of the consumer population to changes in resource density. When $\sigma \gg \lambda$, the steady-state population density is small, thereby increasing the risk of stochastic extinction. On the other hand, as σ decreases, the system will ultimately be poised either near the TC or the Hopf bifurcation (Fig. 1). If the recovery rate ρ is sufficiently small, the TC bifurcation is reached and the resource eventually is eliminated. If ρ exceeds a threshold value, cyclic dynamics will develop as the Hopf bifurcation is approached.

Role of allometry

While there are no a priori constraints on the parameters in the NSM, most organisms correspond to restricted portions of the parameter space. Here we use allometric scaling relations to constrain the covariation of rates in a principled and biologically meaningful manner. Allometric scaling relations highlight common constraints and average trends across large ranges in body size and species diversity. Many of these relations can be derived from a small set of assumptions and below we describe a framework to determine the covariation of timescales and rates

across the range of mammals for each of the key parameters of our model (cf. (38)). We are thereby able to define the regime of dynamics occupied by the entire class of mammals along with the key differences between the largest and smallest mammals. Models explicitly handle storage (45), whereas this feature is implicitly covered by the body fat scaling in our framework.

Nearly all of the rates described in the NSM are determined by consumer metabolism, which can be used to describe the variety of organismal features (39). The scaling relation between an organism's metabolic rate B and its body mass M at reproductive maturity is known to scale as $B = B_0 M^\eta$ (40), where the scaling exponent η is typically close to $2/3$ or $3/4$ for metazoans (e.g., (39)), and has taxonomic shifts for unicellular species between $\eta \approx 1$ in eukaryotes and $\eta \approx 1.76$ in bacteria (3, 41).

Several efforts have shown how a partitioning of B between growth and maintenance purposes can be used to derive a general equation for both the growth trajectories and growth rates of organisms ranging from bacteria to metazoans (3, 42–45). This relation is derived from the simple balance condition

$$B_0 m^\eta = E_m \dot{m} + B_m m,$$

where E_m is the energy needed to synthesize a unit of mass, B_m is the metabolic rate to support an existing unit of mass, and m is the mass of the organism at any point in its development. This balance has the general solution (3, 46)

$$\left(\frac{m(t)}{M}\right)^{1-\eta} = 1 - \left[1 - \left(\frac{m_0}{M}\right)^{1-\eta}\right] e^{-a(1-\eta)t/M^{1-\eta}}, \quad [4]$$

where, for $\eta < 1$, $M = (B_0/B_m)^{1/(1-\eta)}$ is the asymptotic mass, $a = B_0/E_m$, and m_0 is mass at birth, itself varying allometrically as $9.7M^{0.92}$. We now use this solution to define the timescale of reproduction and recovery from starvation (Fig. 2; see (43) for a detailed presentation of these timescales). The time that it takes to reach a particular mass ϵM is given by the timescale

$$\tau(\epsilon) = \ln \left[\frac{1 - (m_0/M)^{1-\eta}}{1 - \epsilon^{1-\eta}} \right] \frac{M^{1-\eta}}{a(1-\eta)}, \quad [5]$$

where we will define values of ϵ to describe a set of rates within our model. For the time to reproduce, $t_\lambda = \tau(\epsilon_\lambda)$, where ϵ_λ is the fraction of the asymptotic mass where an organism is reproductively mature and should be close to one (typically $\epsilon_\lambda \approx 0.95$ (42)). The growth rate is then given by $\lambda = \ln(v)/t_\lambda$ where v is the number of offspring produced, and for any constant value of ϵ_λ this will scale like $\lambda \propto M^{\eta-1}$ for $M \gg m_0$ (3, 42–45).

The rate of recovery $\rho = 1/t_\rho$ requires that an organism accrues sufficient tissue to transition from the hungry to the full state. Since only certain tissues can be digested for energy (for example the brain cannot be degraded to fuel metabolism), we define the rates for starvation, death, and recovery by the timescales required to reach, or return from, specific fractions of the replete-state mass (Fig. 3; see Supporting Information, Table I for parameterizations). We define $m_\sigma = \epsilon_\sigma M$, where $\epsilon_\sigma < 1$ is the fraction of replete-state mass where reproduction ceases. This fraction will be modified if tissue composition systematically scales with adult mass. For example, making use of the observation that body fat in mammals scales with overall body size according to $M_{\text{fat}} = f_0 M^\gamma$ and assuming that once this mass is fully digested the organism starves, this would imply that $\epsilon_\sigma = 1 - f_0 M^\gamma / M$. It follows that the recovery timescale, t_ρ , is the time to go from $m = \epsilon_\sigma \epsilon_\lambda M$ to $m = \epsilon_\lambda M$ (Fig. 2). Using Eqs. [4] and [5] this timescale is given by simply considering an adjusted starting mass of $m'_0 = \epsilon_\sigma \epsilon_\lambda M$, in which case

$$t_\rho = \ln \left[\frac{1 - (\epsilon_\sigma \epsilon_\lambda)^{1-\eta}}{1 - \epsilon^{1-\eta}} \right] \frac{M^{1-\eta}}{a'(1-\eta)} \quad [6]$$

To determine the starvation rate, σ , we are interested in the time required for an organism to go from a mature adult that reproduces at rate λ , to a reduced-mass hungry state where reproduction is impossible. For starving individuals we assume that an organism must meet its maintenance requirements using the digestion of existing mass as the sole energy source. This assumption implies the following simple metabolic balance

$$\dot{m}E'_m = -B_m m \quad [7]$$

$$\dot{m} = -\frac{a'}{M^{1-\eta}} m \quad [8]$$

where E'_m is the amount of energy stored in a unit of existing body mass which differs from E_m , the energy required to synthesize a unit of biomass (45). Given the replete mass, M , of an organism, the above energy balance prescribes the mass trajectory of a non-consuming organism:

$$m(t) = M e^{-a't/M^{1-\eta}}. \quad [9]$$

The time scale for starvation is given by the time it takes $m(t)$ to reach $\epsilon_\sigma M$, which gives

$$t_\sigma = -\frac{M^{1-\eta}}{a'} \ln(\epsilon_\sigma). \quad [10]$$

The starvation rate is then $\sigma = 1/t_\sigma$, which scales with replete-state mass as $1/M^{1-\eta} \ln(1 - f_0 M^\gamma / M)$. An important feature is that σ does not have a simple scaling dependence on λ (Fig. 3), which is important for the dynamics that we later discuss.

The time to death should follow a similar relation, but defined by a lower fraction of replete-state mass, $m_\mu = \epsilon_\mu M$ where $\epsilon_\mu < \epsilon_\sigma$. Suppose, for example, that an organism dies once it has digested all fat and muscle tissues, and that muscle tissue scales with body mass according to $M_{\text{musc}} = u_0 M^\zeta$. This gives $\epsilon_\mu = 1 - (f_0 M^\gamma + u_0 M^\zeta) / M$. Muscle mass has been shown to be roughly proportional to body mass (47) in mammals and thus ϵ_μ is merely ϵ_σ minus a constant. The time to death is the total time to reach $\epsilon_\mu M$ minus the time to starve, or

$$t_\mu = -\frac{M^{1-\eta}}{a'} \ln(\epsilon_\mu) - t_\sigma, \quad [11]$$

and $\mu = 1/t_\mu$.

Although the rate equations [1] are general, here we focus on parameterizations for terrestrial-bound endotherms, specifically mammals, which range from a minimum of $M \approx 1\text{g}$ (the Etruscan shrew *Suncus etruscus*) to a maximum of $M \approx 10^7\text{g}$ (the late Eocene to early Miocene Indricotheriinae). Investigating other classes of organisms would simply involve altering the metabolic exponents and scalings associated with ϵ . Moreover, we emphasize that our allometric equations describe mean relationships, and do not account for the (sometimes considerable) variance associated with individual species.

Stabilizing effects of allometric constraints

As the allometric derivations of the NSM rate laws reveal, starvation and recovery rates are not independent parameters, and the biologically relevant portion of the phase space shown in Fig. 1 is constrained via covarying parameters. Given the parameters of terrestrial endotherms, we find that the starvation

rate σ and the recovery rate ρ are constrained to lie within a small window of potential values (Fig. 4) for the known range of body sizes M . We thus find that the dynamics for all mammalian body sizes are confined to the steady-state regime of the NSM and that limit-cycle behavior is precluded. Incorporating uncertainty in allometric parameters (20% variation around the mean; Fig. 4), we find that, for larger M , the distance to

the TC and Hopf bifurcation decreases. These results suggest that small mammals are marginally less prone to population oscillations—both stable limit cycles and transient cycles—than mammals with larger body size, though starvation and recovery rates across all values of M fall squarely in the steady state for organisms. Above this bound, a number of energetic region at some distance from the Hopf bifurcation, suggesting that cyclic population dynamics should be rare, particularly in environments where resources are limiting.

It should be noted that previous studies have used allometric constraints to explain the periodicity of cyclic populations (48–50), suggesting a period $\propto M^{0.25}$. However this relation seems to hold only for some species (51), and potential drivers range from predator and/or prey lifespans to competitive dynamics (52, 53). Statistically significant support for the existence of population cycles among mammals is relatively rare though predominantly based on time series for small mammals (54). However the longer gestational times and increased difficulty in collecting adequate data precludes obtaining similar-quality information for larger organisms such that testing this particular result is not straightforward.

Extinction risk

Within our model, higher rates of starvation result in a larger flux of the population to the hungry state. In this state reproduction is absent, thus increasing the likelihood of extinction. From the perspective of population survival, it is the rate of starvation relative to the rate of recovery that determines the long-term dynamics of the various species (Fig. 1). We therefore examine the competing effects of cyclic dynamics vs. changes in steady state density on extinction risk as a function of σ and ρ .

To this end, we computed the probability of extinction, where we define extinction as a population trajectory falling below one fifth of the allometrically constrained steady state at any time between $t = 10^5$ and $t \leq 10^8$. This procedure is repeated for 50 replicates of the continuous-time system shown in Eq. 1 for an organism of $M = 100$ grams. In each replicate the initial densities are chosen to be (XF^*, XH^*, R^*) , with X a random variable that is uniformly distributed in $[0, 2]$. By allowing the rate of starvation to vary, we assessed extinction risk across a range of values for σ and ρ between ca. 10^{-7} to 10^{-3} . As expected, higher rates of extinction correlate with both high values of σ if ρ is small, and high values of ρ if σ is small. For low values of σ and high values of ρ , the increased extinction risk results from transient cycles with larger amplitudes as the system nears the Hopf bifurcation (Fig. 5). For high values of σ and low values of ρ , higher extinction risk arises because of the decrease in the steady state consumer population density (Figs. 1B, 5). This interplay creates an ‘extinction refuge’, such that for a constrained range of σ and ρ , extinction probabilities are minimized.

We find that the allometrically constrained values of σ and ρ fall squarely within the extinction refuge (Fig. 5, white point). These values are close enough to the Hopf bifurcation to avoid low steady state densities, and far enough away to avoid large-amplitude transient cycles. The fact that allometric values of σ and ρ fall within this relatively small window supports the possibility that a selective mechanism has constrained the physiological conditions that drive starvation and recovery rates within populations. Such a mechanism would select for organism physiology that generates appropriate σ and ρ values that serve to

Dynamic and energetic barriers to body size

Metabolite transport constraints are widely thought to place strict boundaries on biological scaling (39, 55, 56) and thereby lead to specific predictions on the minimum possible body size for organisms (57). Above this bound, a number of energetic costs and benefits associated with larger body masses, particularly for mammals. One important such example is the *fast-ing endurance hypothesis*, which contends that larger body size, with consequent lower metabolic rates and increased ability to maintain more endogenous energetic reserves, may buffer organisms against environmental fluctuations in resource availability (58). Over evolutionary time, terrestrial mammalian lineages show a significant trend towards larger body size (known as Cope’s rule) (59–62), and it is thought that within-lineage drivers generate selection towards an optimal upper bound of roughly 10^7 grams (59), a value that is likely limited by higher extinction risk for large taxa over longer timescales (60). These trends are thought to be driven by a combination of climate change and niche availability (62); however the underpinning energetic costs and benefits of larger body sizes, and how they influence dynamics over ecological timescales, have not been explored. We argue that the NSM provides a suitable framework to explore these issues.

The NSM correctly predicts that species with smaller masses have larger steady-state population densities (Fig. 6A). Moreover, we show that the NSM provides independent theoretical support for the energy equivalence hypothesis (63, 64). The energy equivalence hypothesis argues that the total energy use, B_{tot} , of a population is constant independent of species size (e.g. (63, 64)). This hypothesis is based on observations showing that the steady state abundance, N^* , of a species is proportional to the inverse of individual metabolism (e.g. $N^* \propto M^{-3/4}/B_0$) (e.g. (63, 64)). This is usually stated as $B_{\text{tot}} = N^*B(M) = Q$ where Q is a constant, and has been shown to hold in both mammalian and vascular plant communities (63, 64). Figure 6A shows that both F^* and H^* scale like $M^{-\eta}$ over a wide range of organism sizes and Figure 6B shows that F^*B is nearly constant over this same range. This result is remarkable because it illustrates that the steady state values of the NSM combined with the derived timescales naturally give rise to the energy equivalence result. Our model shows that the equivalence breaks down at the maximum observed body sizes for mammals, suggesting that this is a hard limit where deviations outside of this range are energetically suboptimal. In the framework of our model, the total metabolic rate of F and H becomes infinite at a finite mass, occurring at the same scale where the steady state resources vanish (Fig. 6). This asymptotic behavior represents an upper bound on mammalian body size and occurs at $M_{\text{max}} = 6.5 \times 10^7$. Moreover, M_{max} , which is entirely determined by the population-level consequences of energetic constraints, is remarkably close to the maximum body size observed in the North American mammalian fossil record (59) as well as the mass predicted from an evolutionary model of body size evolution (60).

It should be noted that this prediction of an asymptotic limit on mammalian size resembles efforts on microbial life where an upper and lower bound on bacterial size, and an upper bound on single cell eukaryotic size, is predicted from similar growth and energetic reasons or from dissimilar

463 scaling of cellular composition which is analogous to the body 527 in the NSM may provide a general within-lineage mechanism
464 fat composition employed here (3, 65). 528 for the evolution of larger body size among terrestrial mammals.

465 We contend that the NSM provides a mechanistic under- 529 The energetics associated with somatic maintenance,
466 standing of the energetic dynamics that give rise to both ob- 530 growth, and reproduction are important elements that influence
467 served limitations on mammalian body size as well as the ob- 531 the dynamics of all populations (11). The NSM is a minimal
468 served trend towards larger body size over evolutionary time. 532 and general model that incorporates the dynamics of starvation
469 The NSM predicts that the steady state resource density R^* 533 and recovery that are expected to occur in resource-limited en-
470 decreases with increasing body size of the consumer popula- 534 vironments. By incorporating allometric relations between the
471 tion (Fig. 6C), and classic resource competition theory predicts 535 rates in the NSM, we found: (i) different organismal masses
472 that the species surviving on the lowest resource abundance will 536 have distinct population dynamic regimes, (ii) allometrically-
473 outcompete others (66–68). Thus, the combined NSM steady- 537 determined rates of starvation and recovery appear to minimize
474 state dynamics and allometric timescales predict that larger 538 extinction risk, and (iii) the dynamic consequences of these rates
475 mammals have an intrinsic competitive advantage given a com- 539 may introduce additional drivers and hard boundaries on the
476 mon resource, but does not offer a within-lineage mechanism by 540 evolution of maximum body size. We suggest that the NSM
477 which larger body sizes are selected for. 541 offers a means by which the dynamic consequences of energetic
478 To examine whether the NSM could provide such a mecha- 542 constraints can be assessed using macroscale interactions be-
479 nism, we begin by noting that a theoretical upper bound on 543 tween and among species. Future efforts will involve exploring
480 mammalian body size is given by $\epsilon_\sigma = 0$, where mammals 544 the consequences of these dynamics in a spatially explicit frame-
481 are entirely composed of metabolic reserves, and this occurs at 545 work, thus incorporating elements such as movement costs and
482 $M = 8.3 \times 10^8$, or $120 \times$ the mass of a male African elephant. 546 spatial heterogeneity, which may elucidate additional tradeoffs
483 Next we examine to what extent a more realistic upper bound 547 associated with the dynamics of starvation and recovery.
484 to body mass may serve as an evolutionary attractor, thus pro-
485 viding a suitable within-lineage mechanism for Cope's rule. We
486 directly assess the susceptibility of an otherwise homogeneous
487 population to invasion by a mutated subset of the population
488 (denoted by ') where individuals have a modified proportion of
489 body fat $M' = M(1 + \chi)$ where $\chi \in [-f_0 M^{\gamma-1}, 0.05]$ (where
490 the lower bound of χ is the proportion of body mass that is
491 not composed of metabolic reserves and the upper bound main-
492 tains the organism's reproductive mass), thus altering the rates
493 of starvation $\sigma(M')$, recovery $\rho(M')$, and the maintenance of
494 both starving $\delta(M')$ and full consumers $\beta(M')$. Importantly,
495 ϵ_σ , which determines the point along the growth curve the de-
496 fines the state of starved foragers, is assumed to remain un-
497 changed for the invader population (see Supplemental Material
498 for detailed derivations of invader rates).

499 To assess the susceptibility of the resident population to
500 invasion, we determine which consumer has a lower steady-
501 state resource density for a given value of χ , again with the
502 expectation that populations able to survive on lower resource
503 densities have a competitive advantage (66). We find that for
504 $M \leq 1.73 \times 10^7$ g, having additional body fat ($\chi > 0$) results in
505 lower steady state resource density ($R^* < R'$), such that the
506 invader has an intrinsic competitive advantage over the resident
507 population. However, for $M > 1.73 \times 10^7$ g, leaner individuals
508 ($\chi < 0$) have lower resource steady state densities, switching
509 the advantage for higher values of M .

510 The observed switch in susceptibility as a function of χ at
511 $M_{\text{opt}} = 1.73 \times 10^7$ g thus serves as an attractor, such that the
512 NSM predicts organismal mass to increase if $M < M_{\text{opt}}$ and
513 decrease if $M > M_{\text{opt}}$. This value is close to but smaller than
514 the asymptotic upper bound for terrestrial mammal body size
515 predicted by the NSM, however it is remarkably close to in-
516 dependent estimates of the largest land mammals, the early
517 Oligocene *Indricotherium* at ca. 1.3×10^7 g and the late Miocene
518 *Deinotherium* at ca. 1.74×10^7 g (61). Additionally, our calcu-
519 lation of M_{opt} as a function of mass-dependent physiological rates
520 is similar to theoretical estimates of maximum body size (60),
521 and provides independent theoretical support for the observa-
522 tion of a 'maximum body size attractor' for North American
523 mammals outlined by Alroy (59). While the state of the envi-
524 ronment, as well as the competitive landscape, will determine
525 whether specific body sizes are selected for or against (62), we
526 propose that the dynamics of starvation and recovery described

548 References

1. Martin TE (1987) Food as a Limit on Breeding Birds: A Life-History Perspective. *Annu. Rev. Ecol. Syst.* 18:453–487.
2. Kirk KL (1997) Life-History Responses to Variable Environments: Starvation and Reproduction in Planktonic Rotifers. *Ecology* 78:434–441.
3. Kempes CP, Dutkiewicz S, Follows MJ (2012) Growth, metabolic partitioning, and the size of microorganisms. *PNAS* 109:495–500.
4. Mangel M, Clark CW (1988) *Dynamic Modeling in Behavioral Ecology* (Princeton University Press, Princeton).
5. Mangel M (2014) Stochastic dynamic programming illuminates the link between environment, physiology, and evolution. *B. Math. Biol.* 77:857–877.
6. Yeakel JD, Dominy NJ, Koch PL, Mangel M (2014) Functional morphology, stable isotopes, and human evolution: a model of consilience. *Evolution* 68:190–203.
7. Morris DW (1987) Optimal Allocation of Parental Investment. *Oikos* 49:332.
8. Tveraa T, Fauchald P, Henaug C, Yoccoz NG (2003) An examination of a compensatory relationship between food limitation and predation in semi-domestic reindeer. *Oecologia* 137:370–376.
9. Daan S, Dijkstra C, Drent R, Meijer T (1988) Food supply and the annual timing of avian reproduction.
10. Jacot A, Valcu M, van Oers K, Kempenaers B (2009) Experimental nest site limitation affects reproductive strategies and parental investment in a hole-nesting passerine. *Animal Behaviour* 77:1075–1083.
11. Stearns SC (1989) Trade-Offs in Life-History Evolution. *Funct. Ecol.* 3:259.
12. Barboza P, Jorde D (2002) Intermittent fasting during winter and spring affects body composition and reproduction of a migratory duck. *J Comp Physiol B* 172:419–434.
13. Threlkeld ST (1976) Starvation and the size structure of zooplankton communities. *Freshwater Biol.* 6:489–496.
14. Weber TP, Ens BJ, Houston AI (1998) Optimal avian migration: A dynamic model of fuel stores and site use. *Evolutionary Ecology* 12:377–401.
15. Mduma SAR, Sinclair ARE, Hilborn R (1999) Food regulates the Serengeti wildebeest: a 40-year record. *J. Anim. Ecol.* 68:1101–1122.

- 591 16. Moore JW, Yeakel JD, Peard D, Lough J, Beere M (2014) 658
 592 Life-history diversity and its importance to population sta- 659
 593 bility and persistence of a migratory fish: steelhead in two 660
 594 large North American watersheds. *J. Anim. Ecol.* 83:1035– 661
 595 1046. 662
- 596 17. Mead RA (1989) in *Carnivore Behavior, Ecology, and Evo-* 663
 597 *lution* (Springer US, Boston, MA), pp 437–464. 664
- 598 18. Sandell M (1990) The Evolution of Seasonal Delayed Im- 665
 599 plantation. *The Quarterly Review of Biology* 65:23–42. 666
- 600 19. Bulik CM, et al. (1999) Fertility and Reproduction in 667
 601 Women With Anorexia Nervosa. *J. Clin. Psychiatry* 668
 602 60:130–135. 669
- 603 20. Trites AW, Donnelly CP (2003) The decline of Steller sea 670
 604 lions *Eumetopias jubatus* in Alaska: a review of the nutri- 671
 605 tional stress hypothesis. *Mammal Review* 33:3–28. 672
- 606 21. Glazier DS (2009) Metabolic level and size scaling of rates 673
 607 of respiration and growth in unicellular organisms. *Funct. 674
 608 Ecol.* 23:963–968. 675
- 609 22. Kooijman SALM (2000) *Dynamic Energy and Mass Bud- 676
 610 gets in Biological Systems* (Cambridge). 677
- 611 23. Sousa T, Domingos T, Poggiale JC, Kooijman SALM 678
 612 (2010) Dynamic energy budget theory restores coherence 679
 613 in biology. *Philos. T. Roy. Soc. B* 365:3413–3428. 680
- 614 24. Diekmann O, Metz JAJ (2010) How to lift a model for in- 681
 615 dividual behaviour to the population level? *Philos. T. Roy. 682
 616 Soc. B* 365:3523–3530. 683
- 617 25. Murdoch WW, Briggs CJ, Nisbet RM (2003) *Consumer- 684
 618 resource Dynamics*, Monographs in population biology 685
 619 (Princeton University Press). 686
- 620 26. Benichou O, Redner S (2014) Depletion-Controlled Starva- 687
 621 tion of a Diffusing Forager. *arXiv*. 688
- 622 27. Bénichou O, Chupeau M, Redner S (2016) Role of Deple- 689
 623 tion on the Dynamics of a Diffusing Forager. 690
- 624 28. Chupeau M, Bénichou O, Redner S (2016) Universality 691
 625 classes of foraging with resource renewal. *Phys. Rev. E* 692
 626 93:032403. 693
- 627 29. Persson L, Leonardsson K, De Roos AM, Gyllenberg M, 694
 628 Christensen B (1998) Ontogenetic Scaling of Foraging Rates 695
 629 and the Dynamics of a Size-Structured Consumer-Resource 696
 630 Model. *Theoretical Population Biology* 54:270–293. 697
- 631 30. Murray JD (2011) *Mathematical Biology: I. An Introduct-* 698
 632 *tion*, Interdisciplinary Applied Mathematics (Springer New 699
 633 York) Vol. 110. 700
- 634 31. Strogatz SH (2008) *Nonlinear Dynamics and Chaos*, With 701
 635 Applications to Physics, Biology, Chemistry, and Engineer- 702
 636 ing (Westview Press). 703
- 637 32. Guckenheimer J, Holmes P (1983) *Nonlinear oscilla- 704
 638 tions, dynamical systems, and bifurcations of vector fields* 705
 639 (Springer, New York). 706
- 640 33. Gross T, Feudel U (2004) Analytical search for bifurcation 707
 641 surfaces in parameter space. *Physica D* 195:292–302. 708
- 642 34. Hastings A (2001) Transient dynamics and persistence of 709
 643 ecological systems. *Ecol. Lett.* 4:215–220. 710
- 644 35. Neubert M, Caswell H (1997) Alternatives to resilience for 711
 645 measuring the responses of ecological systems to perturba- 712
 646 tions. *Ecology* 78:653–665. 713
- 647 36. Caswell H, Neubert MG (2005) Reactivity and transient 714
 648 dynamics of discrete-time ecological systems. *Journal of 715
 649 Difference Equations and Applications* 11:295–310. 716
- 650 37. Neubert M, Caswell H (2009) Detecting reactivity. *Ecology*. 717
- 651 38. Yodzis P, Innes S (1992) Body Size and Consumer-Resource 718
 652 Dynamics. *Am. Nat.* 139:1151–1175. 719
- 653 39. Brown J, Gillooly J, Allen A, Savage V, West G (2004) To- 720
 654 ward a metabolic theory of ecology. *Ecology* 85:1771–1789. 721
- 655 40. West GB, Woodruff WH, Brown JH (2002) Allometric scal- 722
 656 ing of metabolic rate from molecules and mitochondria to 723
 657 cells and mammals. *Proc. Natl. Acad. Sci. USA* 99 Suppl 724
41. DeLong JP, Okie JG, Moses ME, Sibly RM, Brown JH 1:2473–2478.
 42. (2010) Shifts in metabolic scaling, production, and effi-
 43. ciency across major evolutionary transitions of life. *PNAS*
 107:12941–12945.
44. West GB, Brown JH, Enquist BJ (2001) A general model 42
 45. for ontogenetic growth. *Nature* 413:628–631.
46. Moses ME, et al. (2008) Revisiting a Model of Ontogenetic 43
 47. Growth: Estimating Model Parameters from Theory and 44
 48. Data. <http://dx.doi.org.proxy.lib.sfu.ca/10.1086/679735>
 171:632–645.
49. Gillooly JF, Charnov EL, West GB, Savage VM, Brown JH 44
 50. (2002) Effects of size and temperature on developmental 45
 51. time. *Nature* 417:70–73.
52. Hou C, et al. (2008) Energy Uptake and Allocation During 45
 53. Ontogeny. *Science* 322:736–739.
54. Bettencourt LMA, Lobo J, Helbing D, Kuhnert C, West 46
 55. GB (2007) Growth, innovation, scaling, and the pace of life 47
 56. in cities. *Proc. Natl. Acad. Sci. USA* 104:7301–7306.
57. Folland JP, Mc Cauley TM, Williams AG (2008) Allometric 48
 58. scaling of strength measurements to body size. *Eur J 49
 59. Appl Physiol* 102:739–745.
60. Calder III WA (1983) An allometric approach to population 48
 61. cycles of mammals. *J. Theor. Biol.* 100:275–282.
62. Peterson RO, Page RE, Dodge KM (1984) Wolves, Moose, 49
 63. and the Allometry of Population Cycles. *Science* 224:1350– 50
 64. 1352.
65. Krukonis G, Schaffer WM (1991) Population cycles in mam- 50
 66. mals and birds: Does periodicity scale with body size? *J. 51
 67. Theor. Biol.* 148:469–493.
68. Hendriks AJ, Mulder C (2012) Delayed logistic and Rosen- 51
 69. zweig-MacArthur models with allometric parameter setting 52
 70. estimate population cycles at lower trophic levels well. *Eco- 53
 71. logical Complexity* 9:43–54.
72. Kendall BE, et al. (1999) Why do populations cycle? A syn- 52
 73. thesis of statistical and mechanistic modeling approaches. 53
 74. *Ecology* 80:1789–1805.
75. Höglstedt G, Seldal T, Breistøl A (2005) Period length in 54
 76. cyclic animal populations. *Ecology* 86:373–378.
77. Kendall, Prendergast, Bjornstad (1998) The macroecology 55
 78. of population dynamics: taxonomic and biogeographic pat- 54
 79. terns in population cycles. *Ecol. Lett.* 1:160–164.
80. Brown J, Marquet P, Taper M (1993) Evolution of body 55
 81. size: consequences of an energetic definition of fitness. *Am. 56
 82. Nat.* 142:573–584.
83. West GB, Brown JH, Enquist BJ (1997) A General Model 56
 84. for the Origin of Allometric Scaling Laws in Biology. *Sci- 57
 85. ence* 276:122–126.
86. West GB, Woodruff WH, Brown JH (2002) Allometric scal- 57
 87. ing of metabolic rate from molecules and mitochondria to 58
 88. cells and mammals. *Proc. Natl. Acad. Sci. USA* 99:2473– 59
 89. 2478.
90. Millar J, Hickling G (1990) Fasting Endurance and the 58
 91. Evolution of Mammalian Body Size. *Funct. Ecol.* 4:5–12.
92. Alroy J (1998) Cope's rule and the dynamics of body 59
 93. mass evolution in North American fossil mammals. *Science* 280:731.
94. Clauset A, Redner S (2009) Evolutionary Model of Species 60
 95. Body Mass Diversification. *Phys. Rev. Lett.* 102:038103.
96. Smith FA, et al. (2010) The Evolution of Maximum Body 61
 97. Size of Terrestrial Mammals. *Science* 330:1216–1219.
98. Saarinen JJ, et al. (2014) Patterns of maximum body size 62
 99. evolution in Cenozoic land mammals: eco-evolutionary pro- 63
 100. cesses and abiotic forcing. *Proc Biol Sci* 281:20132049– 64
 101. 20132049.
102. Allen AP, Brown JH, Gillooly JF (2002) Global Biodiver- 63
 103. sity, Biochemical Kinetics, and the Energetic-Equivalence 65
 104. 66

- 725 Rule. *Science* 297:1545–1548.
- 726 64. Enquist BJ, Brown JH, West GB (1998) Allometric scal- 727 ing of plant energetics and population density : Abstract : 728 *Nature*. *Nature* 395:163–165.
- 729 65. Kempes CP, Wang L, Amend JP, Doyle J, Hoehler T (2016) 730 Evolutionary tradeoffs in cellular composition across diverse 731 bacteria. *ISME J* 10:2145–2157.
- 732 66. Tilman D (1981) Tests of Resource Competition Theory Us- 733 ing Four Species of Lake Michigan Algae. *Ecology* 62:802– 734 815.
- 735 67. Dutkiewicz S, Follows MJ, Bragg JG (2009) Modeling the 736 coupling of ocean ecology and biogeochemistry. *Global Bio- 737 geochem. Cycles* 23:1–15.
- 738 68. Barton AD, Dutkiewicz S, Flierl G, Bragg J, Follows MJ 739 (2010) Patterns of Diversity in Marine Phytoplankton. *Sci- 740 ence* 327:1509–1511.

741 **ACKNOWLEDGMENTS.** We thank Luis Bettencourt, Jean Philippe Gibert, 742 Eric Libby, and Seth Newsome for helpful discussions and comments on the 743 manuscript. J.D.Y. was supported by startup funds at the University of California, 744 Merced, and an Omidyar Postdoctoral Fellowship at the Santa Fe Institute. C.P.K. 745 was supported by an Omidyar Postdoctoral Fellowship at the Santa Fe Institute. 746 S.R. was supported by grants DMR-1608211 and 1623243 from the National 747 Science Foundation, and by the John Templeton Foundation, all at the Santa Fe 748 Institute.

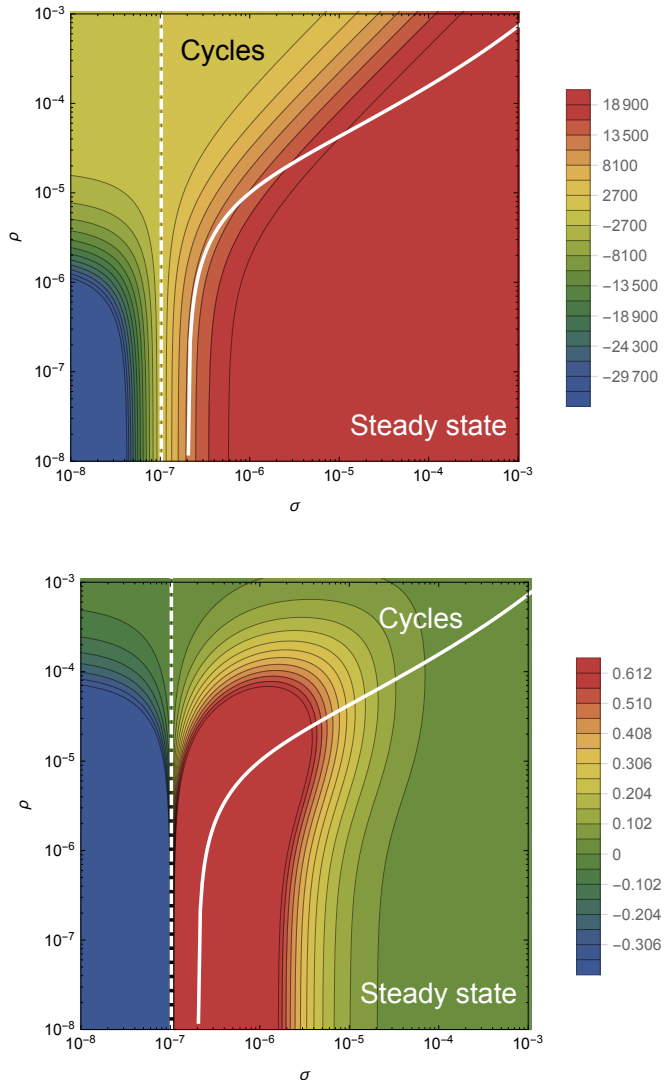


Fig. 1: The transcritical (dashed) and Hopf bifurcation (solid) as a function of the starvation rate σ and recovery rate ρ for a 100g consumer. These bifurcation conditions separate parameter space into infeasible, cyclic, and steady state dynamic regimes. The color gradient shows the steady state densities for (A) the resource R^* and the (B) energetically replete consumers F^* , (warmer colors denote higher densities). Steady state densities for the energetically deficient consumers H^* (not shown) scale with those for F^* .

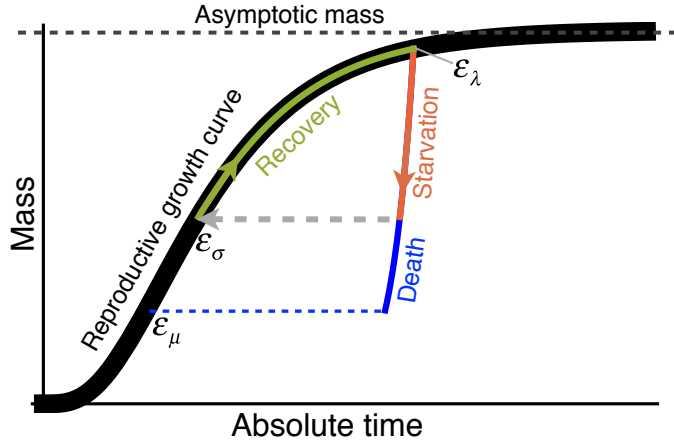


Fig. 2: The growth trajectory over absolute time of an individual organism as a function of body mass. Initial growth follows the black trajectory to an energetically replete reproductive adult mass $m = \epsilon_\lambda M$ which we assume is 95% asymptotic mass M . Starvation follows the red trajectory to $m = \epsilon_\sigma \epsilon_\lambda M$, and recovery follows the green growth trajectory to the replete adult mass. Alternatively, death from starvation follows the blue trajectory to $m = \epsilon_\mu \epsilon_\lambda M$.

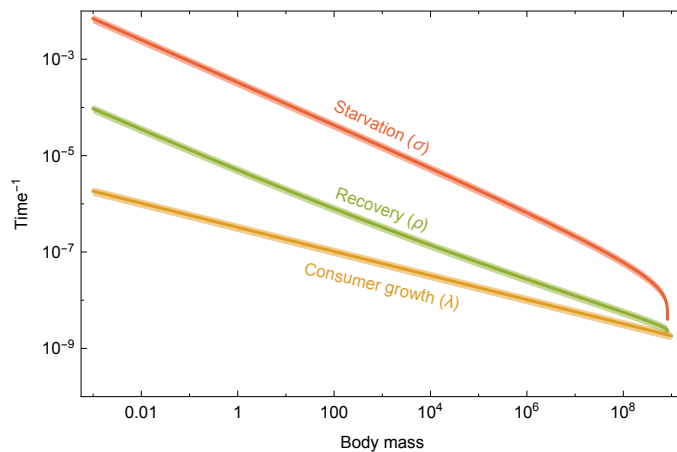


Fig. 3: Allometrically constrained starvation rate σ (red) and recovery rate ρ (green) relative to the reproductive rate λ (orange) as a function of body mass. The rate of starvation is greater than the rate of reproduction for all realized terrestrial endotherm body sizes. Mean values $\pm 20\%$ variation are shown by the shaded region for each rate.

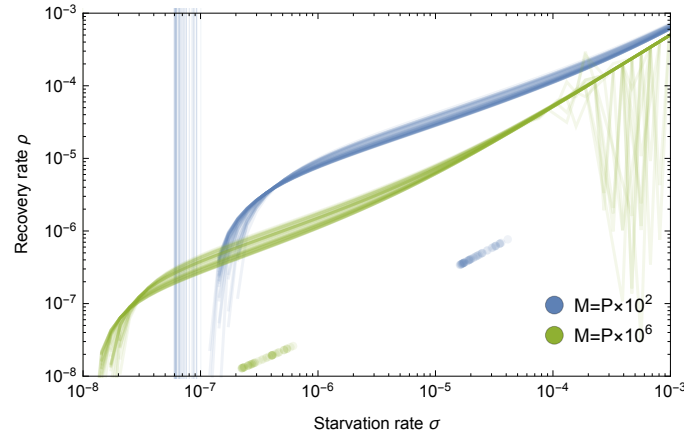


Fig. 4: Transcritical (vertical lines) and Hopf bifurcations (curves) for allometrically determined starvation σ and recovery ρ rates as a function of different mammalian body sizes: $M = P \times 10^2\text{g}$ (blue) and $M = P \times 10^6\text{g}$ (green), where P is a random uniform variable in $[1, 9]$. Points denote realized values of σ and ρ given the drawn values for M .

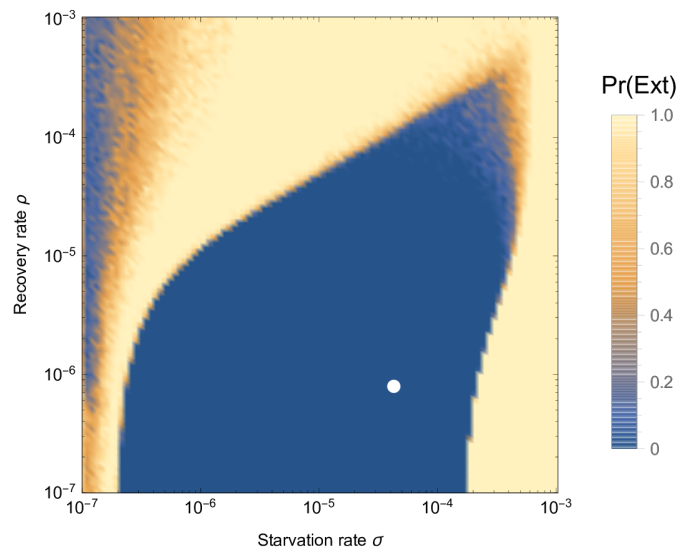


Fig. 5: Probability of extinction for a 100g consumer as a function of the starvation rate σ and recovery rate ρ , where the initial density is given as $A(F^*, H^*, R^*)$, with A being a random uniform variable in $[0, 2]$. Extinction is defined as the population trajectory falling below $0.1 \times$ the allometrically constrained steady state. The white point denotes the allometrically constrained starvation and recovery rate.

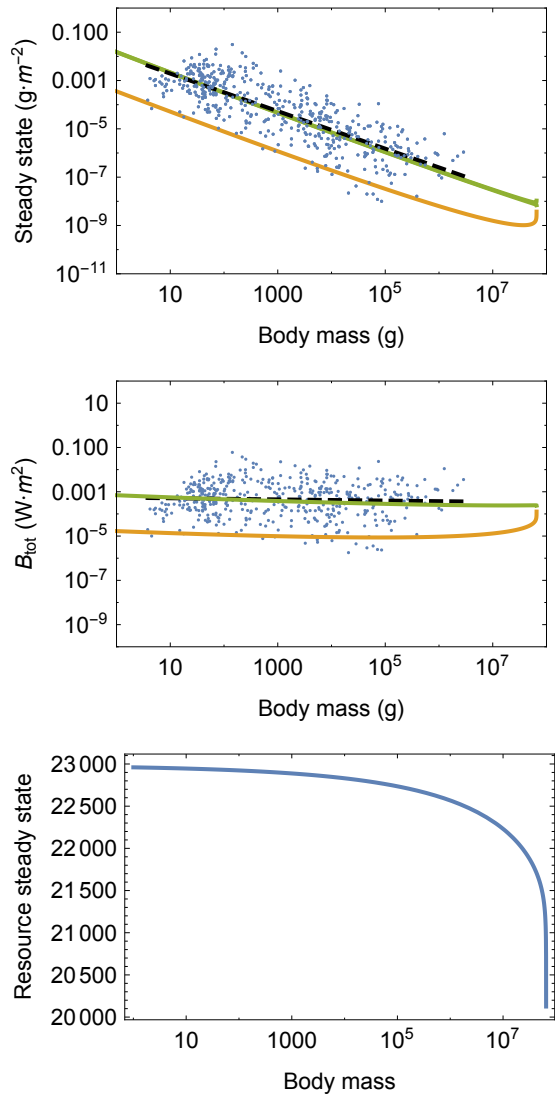


Fig. 6: (A) Consumer steady states F^* (green) and H^* (orange) as a function of body mass. (B) Total energetic use B_{tot} of consumer populations at the steady state as a function of body mass. (C) Resource steady state R^* as a function of consumer body mass.

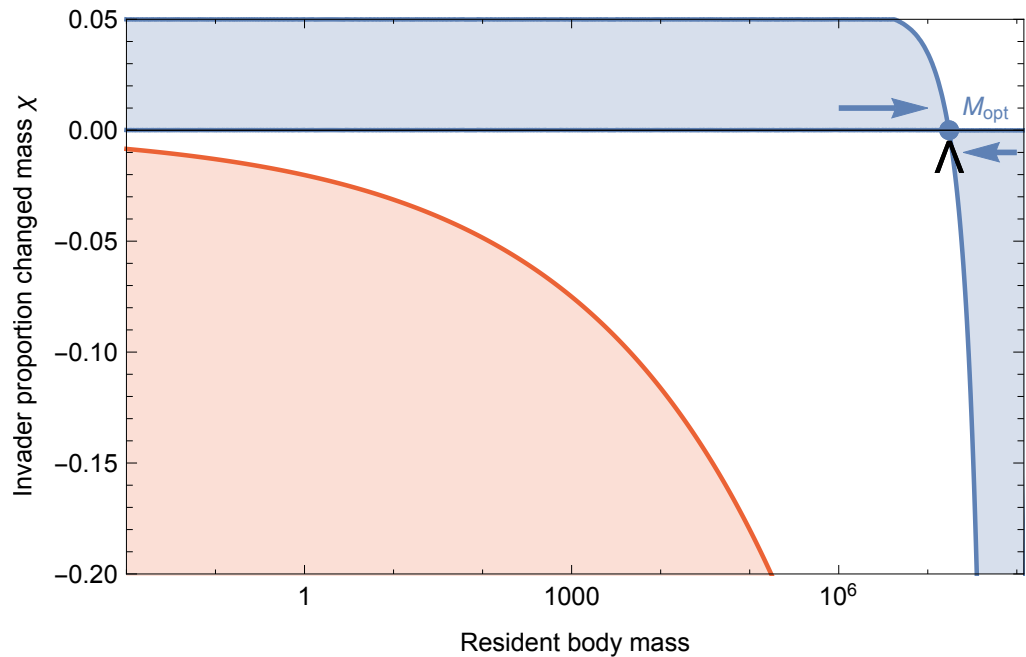


Fig. 7: Invasion feasibility for organisms with a proportional change in mass χ against a population with a resident body mass M . The blue region denotes proportions of modified mass χ resulting in successful invasion. The red region denotes values of χ that result in a mass that is below the starvation threshold and is thus infeasible. Arrows point to the predicted optimal mass $M_{\text{opt}} = 1.73 \times 10^7$, which serves as an evolutionary attractor for body mass. The black wedge points to the largest body mass known for terrestrial mammals at 7.4×10^7 g (61).